

Exploiting Implicit Rigidity Constraints via Weight-Sharing Aggregation for Scene Flow Estimation from Point Clouds

Yun Wang [†]

wangyun@hust.edu.cn

Cheng Chi [†]

chengchi.hust@gmail.com

Xin Yang 

xinyang2014@hust.edu.cn

Abstract

Scene flow estimation, which predicts the 3D motion of scene points from point clouds, is a core task in autonomous driving and many other 3D vision applications. Existing methods either suffer from structure distortion due to ignorance of rigid motion consistency or require explicit pose estimation and 3D object segmentation. Errors of estimated poses and segmented objects would yield inaccurate rigidity constraints and in turn mislead scene flow estimation. In this paper, we propose a novel weight-sharing aggregation (WSA) method for feature and scene flow up-sampling. WSA does not rely on estimated poses and segmented objects, and can implicitly enforce rigidity constraints to avoid structure distortion in scene flow estimation. To further exploit geometric information and preserve local structure, we design a deformation degree module aim to keep the local region invariance. We modify the PointPWC-Net and integrate the proposed WSA and deformation degree module into the enhanced PointPWC-Net to derive an end-to-end scene flow estimation network, called WSAFlowNet. Extensive experimental results on the FlyingThings3D [19] and KITTI [21] datasets demonstrate that our WSAFlowNet achieves the state-of-the-art performance and outperforms previous methods by a large margin. We will release the source code at <https://github.com/wangyunlhr/WSAFlowNet.git>

State-of-the-art scene flow estimation methods [24, 34, 36] are mainly based on the 3D point convolution neural networks (CNNs), such as PointNet [25] and PointNet++ [26]. For instance, FlowNet3D [17] designs an end-to-end scene flow estimation network based on PointNet++ and introduces a flow embedding layer to encode 3D motion between the source and target point clouds. PointPWC-Net [36] adopts PointConv [35] as the convolution operation and introduces a coarse-to-fine strategy to improve the accuracy, in particular for points with large displacements. The pipeline: it first estimates the scene flow at the coarsest resolution and then operates layer-by-layer refinement to the highest resolution. Between the adjacent layers, it operates the process of upsampling layer, which propagates the estimated information from coarser layer to finer layer. To balance accuracy and computational efficiency, there are several methods [3, 29, 30] employ coarse-to-fine structure in scene flow estimation task. Despite the success of these works, they ignore the fact that the scene flow for points of the same rigid object should conform to the same geometric transformation, i.e., rigid motion consistency. As a result, these methods could suffer from rigid structure distortion in the scene flow estimation.

To solve above problem, we propose a network that utilizes implicit rigidity constraints based on the coarse-to-fine architecture. We focus on the internal relations within the point's neighborhood $N(p_i)$. First, we propose a weight-sharing aggregation approach which is utilized in the up-sampling layer and implicitly enforces the rigidity constraints to avoid structure distortion in scene flow estimation. Importantly, our method does not require explicit rigid object clustering/segmentation or pose estimation, which helps to avoid error interference that may arise from combining multiple tasks. The key idea of weight-sharing aggregation is grounded in our mathematical proof that for any 3D point p_i and its neighboring points $N(p_i)$, using identical weights to aggregate the point coordinates of $N(p_i)$, along with their features of $N(p_i)$ and the scene flow of $N(p_i)$ can enforce consistent motion implicitly for points in $N(p_i)$. Furthermore, we propose a deformation degree module which measures the deformation degree of lo-

1. Introduction

Estimating the 3D motion of scene points from two consecutive frames, known as scene flow estimation, is vital to many 3D applications including autonomous driving [2, 23, 38] and point clouds segmentation [6]. Traditional methods usually estimate scene flow from RGB or RGB-D images [4, 20, 22, 27, 33]. Recently, due to the increasing application of 3D sensors such as LiDAR, directly estimating scene flow from 3D point clouds has attracted a lot of interests.

[†] Equal contribution.  Corresponding author.

cal structure between the reference points $N(p_i)$ and the warped points $N(p_i^w)$. It is constructed using the source point cloud and predicted scene flow, to further enhance local structure consistency. The deformation degree module serves as an additional input for our estimator providing supplementary geometric information. We build a scene flow estimation network, named WSAFlowNet, by integrating our weight-sharing aggregation and deformation degree module into an enhanced version of PointPWC-Net [36]. Extensive experimental results demonstrate the effectiveness and generalization capability of our method. Our method surpasses the current state-of-the-art methods Bi-PointFlowNet [3]. According to the EPE3D metric, we outperform Bi-PointFlowNet by 14.6% on the FlyingThings3D [19] dataset, and by 7.6% on the KITTI [21] dataset.

In summary, this paper makes three contributions:

1. A novel weight-sharing aggregation approach for up-sampling which implicitly enforces rigidity constraints by using identical weights for aggregation of point coordinates, scene flow and features. We mathematically and experimentally prove the feasibility of our approach. In addition, our approach does not require explicit pose estimation and/or 3D object segmentation.
2. A deformation degree module which captures the discrepancy in local structure between the source point cloud and the warped point cloud. This module helps to preserve the local structure of rigid objects during scene flow estimation.
3. An effective scene flow estimation network, named WSAFlowNet, which integrates these two approaches to achieve the state-of-the-art performance on the FlyingThings3D and KITTI benchmarks.

2. Related Work

Scene flow estimation. Several recent methods have achieved impressive performance on the scene flow estimation task [1, 11, 31, 32, 36]. PointPWC-Net [36] introduces a coarse-to-fine network architecture to estimate scene flow. It can capture large motions without enlarging the scope of search. Additionally, it proposes a novel patch-to-patch cost volume to encode point motions effectively. RMS-FlowNet [1], on the other hand, designs a Patch-to-Dilated-Patch flow embedding block that, in conjunction with Random-sampling, allows for operation on large-scale point clouds. PV-RAFT [34] constructs point-voxel correlation fields to capture all-pairs relations. Focusing on the irregularity of point cloud, RCP [10] proposes a method that applies pointwise optimization on 3D flows first and then integrates regular information into the recurrent network to achieve global regularization. The methods mentioned above only use unidirectional features, which can result in insufficient information. To address this limitation, Bi-PointFlowNet [3] introduces bidirectional flow embedding layers to ex-

tract correlations both forward and backward. 3DFlow [29] proposes an all-to-all flow embedding layer that can capture distant points and combine them with backward reliability validation. However, this pointwise scene flow estimation method does not make full use of structural information during movement. Consequently, they may encounter structure distortion in some challenging scenes, which is often caused by the sparsity of point clouds.

Rigidity constraints. A straightforward solution to prevent structure distortion is to explicitly estimate geometric transformations of rigid objects in a scene and enforce rigid motion consistency on estimated scene flows. To this end, Gojcic et al. [9] categorize scene points into the foreground clusters, which consist of several rigid objects, and the background cluster. They then compute the ego-motion and the geometric transformation of each object between the source and target point clouds via [5, 14, 37]. Next, they enforce the estimated scene flows of the same object to conform to the same geometric transformation. Dong et al. [7] also adopt a similar approach, where they generate an abstraction mask for each input source point cloud using a pre-trained segmentation network [9] and the DBSCAN clustering algorithm [8]. They then estimate poses for each object using [14]. After that, direct multi-body rigidity constraints are computed based on the abstraction mask and poses. These constraints are then integrated into the recurrent neural network to alleviate structure distortion in scene flow estimation. To alleviate inevitable errors in 3D object segmentation, HCRF-Flow [16] treats spatially neighboring points as a rigid object and employs a conditional random fields (CRF [28]) to enforce local smoothness and rigid motion consistency. However, all the aforementioned methods require explicit pose estimation, which is also very challenging. Inevitably errors in pose estimation can lead to inaccurate constraints and in turn mislead scene flow estimation.

3. Method

Fig. 1. shows an overview (§ 3.1) of our WSAFlowNet which consists of two important components, weight-sharing aggregation module and deformation degree module, that play significant roles in the process of scene flow refinement. In the following, we first explain the proposed weight-sharing aggregation module in detail (§ 3.2). Then, we describe the construction of Deformation degree module (§ 3.3). Finally, we discuss how to modify the network architecture and present implementation details of the proposed modules (§ 3.4).

3.1. Overview

The inputs of our network are two sets of point clouds $P = \{p_i \in \mathbb{R}^3\}_{i=1}^{N_1}$ at timestamp t and $Q = \{q_i \in \mathbb{R}^3\}_{i=1}^{N_2}$ at timestamp $t+1$. Our goal is to estimate the scene flow

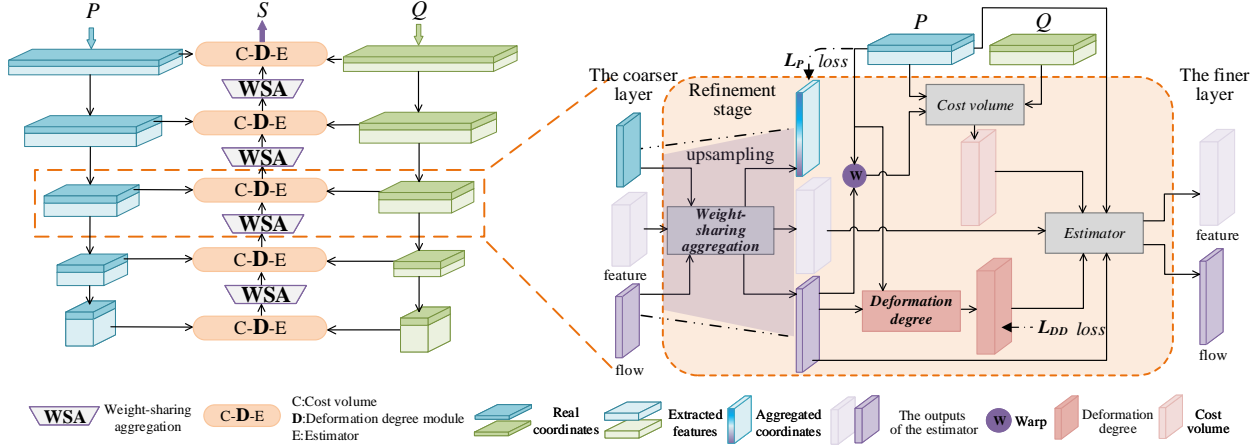


Figure 1. **WSAFlowNet overview.** The left side illustrates the entire pipeline of the coarse-to-fine network. The inputs of the network are two consecutive sets of point clouds P, Q , and output the scene flow corresponding to the P . There are three main processes, including feature abstraction, cost volume construction, and the refinement of scene flow. The right side highlights **the refinement process**, we design two important modules, i.e. **weight-sharing aggregation** (Fig. 2) and **deformation degree module** (Fig. 3). Weight-sharing aggregation realizes the upsampling operation. Deformation degree module captures the discrepancy in local structure between the source point cloud and the warped point cloud. It also acts as the input of the estimator to supply sufficient geometric information.

$S = \{s_i \in \mathbb{R}^3\}_{i=1}^{N_1}$ for every $p_i \in P$. Due to the sparsity of point cloud data, P and Q are not exactly corresponding, so the relationship between P, Q , and S can only be expressed approximately, which is represented by $P + S \approx Q$. We also assume that the majority of local regions satisfy the approximately rigid assumption as described in HCRF-Flow [16], [18]. The motion of points within the local area follows the same transformation defined as $R \in SO(3)$ and $t \in \mathbb{R}^3$.

We adopt the coarse-to-fine structure PointPWC-Net [36] as the baseline. First, we construct feature pyramid for point clouds P and Q . Next, based on the extracted feature, we conduct the scene flow estimation in the coarsest layer and then operate the layer-by-layer refinement to the finest layer. Between adjacent layers, we apply upsampling layer based on weight-sharing aggregation. The upsampled scene flow will be propagated to the finer layer by warping, which will enable the adjustment of the search center for matching. The upsampled feature will be fed into the scene flow estimator to supply movement information. At each layer, we perform the four operations warping layer, cost volume construction, deformation degree module, scene flow estimator sequentially.

3.2. Weight-sharing aggregation module

In scene flow estimation task, due to the sparsity of point cloud data, the point clouds from two consecutive frames are not one-to-one correspondence. This results in matching errors and causes the warped point clouds to undergo structural deformation. To alleviate the problem of mismatch, we

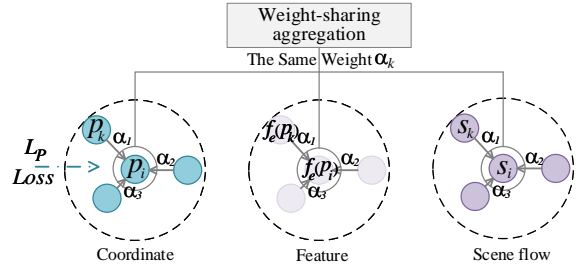


Figure 2. **Weight-sharing aggregation.** During the upsampling process, the weights among point coordinates, features and scene flow are consistent. $f_e(p_i)$ and s_i are the feature and scene flow corresponding to p_i .

propose a weight-sharing aggregation module that utilizing implicit rigidity constraints during the upsampling process.

In the upsampling process, weight aggregation is a common implementation that involves assigning different weights to the information of neighboring points in a coarser layer in order to compute the information of the central point in a finer layer. In this paper, we design a weight-sharing aggregation module which implicitly enforces rigidity constraints by considering the relationship between coordinates, features, and scene flow.

According to rigidity constraints (points on the same object have the same motion (R, t)) and the definition of scene flow, the scene flow aggregation process corresponding to each point should be consistent with the coordinate aggregation process of the point, that is, weight-sharing, as shown in Eq. (1-6). In addition, feature is an intermediate quan-

tity closely related to scene flow and point coordinates, so we extend the weight sharing to the feature level, namely Eq. (7). In specific implementation, WSA module is applied in the upsampling process of refinement stage. In addition to weight-sharing, the coordinate loss Eq. (18) is also added to constrain the weights for aggregation. This transforms the weights' equation solving problem into a regression problem, which ensure that interpolated coordinates are consistent with the ground truth, and then the corresponding scene flow will be close to the target value.

By introducing the aggregation process of point coordinates, weight-sharing aggregation helps to constrain the aggregation process of features. Moreover, it contains the condition that points on the same object conform to the same motion and implicitly enforces rigidity constraints, which reduces the impact of mismatch. Most existing methods [29, 30] don't involve point coordinates upsampling, and they perform the independent upsampling process for feature and scene flow.

The weight-sharing aggregation constraints. In the local rigid region where the points inside have the same movement (R, t) , if aggregated weight α_k satisfies both Eq. (1) and Eq. (2), then it can derive Eq. (3) related to the aggregation of scene flow.

Conditions:

$$\sum_{k=1}^K \alpha_k = 1 \quad (1)$$

$$\sum_{k=1}^K \alpha_k p_k = p_i \quad (2)$$

Conclusion:

$$\sum_{k=1}^K \alpha_k s_k = s_i \quad (3)$$

Where $p_k \in N(p_i)$, $N(p_i)$ is defined as the group of K nearest neighbors of p_i , determined by their distance from p_i . The constant K can be set to any value as required, which represents the size of the neighborhood. s_i is the predicted scene flow of point p_i .

Proof:

Utilize R, t to denote the motion of p_k as Eq. (4).

$$T(p_k) = Rp_k + t \quad (4)$$

According to the definition of scene flow, aggregation of S is explicitly expressed as:

$$s_k = T(p_k) - p_k = (R - I)p_k + t \quad (5)$$

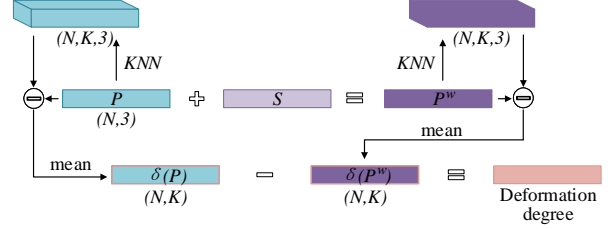


Figure 3. **Deformation degree module.** Calculation of the neighborhood relationship among the point and the neighborhood points is illustrated in the upper part. Then we compare the neighborhood relationship between the source point cloud's $\delta(P)$ and the warped point cloud's $\delta(P^w)$.

$$\begin{aligned} \sum_{k=1}^K \alpha_k s_k &= \sum_{k=1}^K \alpha_k \{(R - I)p_k + t\} \\ &= (R - I) \sum_{k=1}^K \alpha_k p_k + t \sum_{k=1}^K \alpha_k \\ &= (R - I)p_i + t \\ &= s_i \end{aligned} \quad (6)$$

We infer that the feature, intermediate variable between point cloud and scene flow, should have a matching consistency relationship.

Corresponding equation goes here:

$$\sum_{k=1}^K \alpha_k f_e(p_k) = f_e(p_i) \quad (7)$$

where $f_e(p_i)$ denotes the output feature of scene flow estimator for point p_i .

3.3. Deformation degree module

In addition to using (R, t) to make rigidity constraints according to the definition of scene flow, another way to implement rigidity constraints is to maintain local structure invariance in scene flow estimation task. Laplacian regularization [15, 16, 36] utilize the Laplacian coordinate vector to represent the local structure, which computing the average value of the direction vector between the center point and the neighborhood points. Then it adds loss to constrain the warped point P^w to have the same local structure with Q .

We propose a novel module named deformation degree module to maintain local rigid structure invariance, which provides a stronger loss constraint. Firstly, we construct a variable δ to represent the local structure, calculating the distance between the central point and the K nearest neighborhood points in the local rigid area. In contrast to Laplacian regularization, we maintain the dimension of K to enforce a one-to-one structural relationship between the central point and its neighborhood points. Secondly, we calculate the difference δ_{DD} between $\delta(P)$ and $\delta(P^w)$. There is

a priori knowledge that the distance between any two points should remain constant in a local rigid region, even as the objects in the scene undergo motion. Therefore, we enforce a loss to make the difference δ_{DD} converge to 0 to preserve the local structure and we input the δ_{DD} into scene flow estimator to supplement the geometric information. In this way, we utilize the stronger prior information to reducing rigid objects’ local deformation.

$$p_i^w = p_i + s_i \quad (8)$$

$$\delta(P) = \left\{ \frac{1}{C} |p_k - p_i| \mid p_k \in N(p_i) \right\} \quad (9)$$

$$\delta(P^w) = \left\{ \frac{1}{C} |p_k^w - p_i^w| \mid p_k^w \in N(p_i^w) \right\} \quad (10)$$

$$\delta_{DD} = |\delta(P) - \delta(P^w)| \quad (11)$$

where p_i^w represents the warped point. $N(p_i)$, $N(p_i^w)$ represents the neighborhood centered on p_i and p_i^w respectively. C indicates the number of channels.

3.4. Network Architecture

We adopt PointPWC-Net [36] as our baseline, equip it with our proposed module, and modify the network structure. The pipeline is a coarse-to-fine structure. It first estimates the scene flow at the lowest resolution and then refine several times to the highest resolution. The main processes consist of upsampling layer based on the weight-sharing aggregation, warping layer, cost volume, deformation degree module, scene flow estimator. The implementation details are described as follows.

Feature pyramid. We adopt the *set_conv* layer proposed by FlowNet3D [17] to encode feature and downsample $l-1$ layer to l layer by Farthest Point Sampling. Our pyramid structure has five levels $\{l_0 - l_4\}$ by adding a layer for estimating at the roughest resolution (1/128 of the input scale), so that doesn’t cause a lot of memory consumption. For the l_3 level, adding a rougher layer to provide scene flow initialization for cost volume construction is better than operating it directly.

WSA in the upsampling layer. Upsampling layer is a process of interpolating the coordinates, features, and scene flow from a coarse layer to a finer layer. Our WSA module involves using a consistent weighted aggregation method for all three components, and we will focus on the features as an example. For each point p_i^{l-1} in the finer level $l-1$, we select its K nearest neighbors p_k^l in the coarser level l ,

denoted by $p_k^l \in N(p_i^{l-1})$. The upsampling process for features are formulated as follows.

$$\alpha_k = \text{softmax} \left(\text{mean} \left(\text{MLP} \left([p_k^l - p_i^{l-1}, f_e(p_k^l)] \right) \right) \right) \quad (12)$$

$$f_e(p_i^{l-1}) = \sum_{k=1}^K \alpha_k f_e(p_k^l) \quad (13)$$

where $[\cdot, \cdot]$ indicates concatenation operation. $\text{mean}()$ indicates operating the average operation in the channel dimension. $f_e(p_i^l)$ denotes the output feature of scene flow estimator for point p_i^l .

Then we reuse α_i for upsampling coordinates, scene flow and add the coordinate loss. Other methods doesn’t involve point coordinates upsampling and the common process of upsampling feature and scene flow is performed separately.

Warping layer. We use the upsampled scene flow from the coarser layer to warp the point cloud p_i in the finer layer.

$$(p_i^w)^{l-1} = p_i^{l-1} + \text{up}(s_i^l) \quad (14)$$

where $\text{up}()$ indicates WSA upsampling process.

Cost volume. We construct the cost volume between the warped source point P^w and the target point Q , which reduces the search area. We adopt patch-to-dilated-patch cost volume to enlarge the receptive field, following RMS-FlowNet [1].

Deformation degree module. First, computing the distance between two points to represent the local structure for P and P^w . Second, measuring the difference between $\delta(P)$ and warped $\delta(P^w)$, which is deformation degree module. Note that, δ_{DD} does not contain learnable parameters and it will be inputted into the estimator as the supplement of geometric information.

Scene flow estimator. The input to the scene flow estimator consists of five components: the feature $f^{l-1}(p_i)$ of point cloud p_i , cost volume CV_i , deformation degree module δ_{DD_i} , the upsampled output feature of estimator in the coarse layer $\text{up}(f_e^l)$, the upsampled scene flow $\text{up}(s^l)$. Inspired by DenseNet [13], we adopts feature reuse and bypass set in scene flow estimator. The output feature of estimator $f_e^{l-1}(p_i)$ which represents the flow motion information and the predicted scene flow are as follows.

$$f_e^{l-1}(p_i) = \text{MLP} \left([f^{l-1}(p_i), CV_i, \delta_{DD_i}, \text{up}(f_e^l(p_i)), \text{up}(s_i^l)] \right) \quad (15)$$

$$s_i^{l-1} = FC(f_e^{l-1}(p_i)) \quad (16)$$

where $f_e^{l-1}(p_i)$ denotes the output feature of the estimator. s_i^{l-1} denotes the predicted scene flow. $[\cdot, \cdot]$ indicates concatenation operation. $\text{up}()$ indicates WSA upsampling process. FC denotes fully connected layer.

Dataset	Method	EPE3D(m)↓	Acc3D Strict↑	Acc3D Relax↑	Outliers3D↓	EPE2D↓	Acc2D↑
FlyingThings3D [19]	PointPWC-Net [36]	0.0588	0.7379	0.9276	0.3424	3.2390	0.7994
	RMS-FlowNet [1]	0.0560	0.7920	0.9550	0.3240	-	-
	HCRF-Flow [16]	0.0488	0.8337	0.9507	0.2614	2.5652	0.8704
	PV-RAFT [34]	0.0461	0.8169	0.9574	0.2924	-	-
	FlowStep3D [15]	0.0455	0.8162	0.9614	0.2165	-	-
	RCP [10]	0.0403	0.8567	0.9635	0.1976	-	-
	Bi-PointFlowNet [3]	0.0280	0.9180	0.9780	0.1430	1.5820	0.9290
	3DFlow [29]	0.0281	0.9290	0.9817	0.1458	1.5229	0.9279
	Ours	0.0239	0.9391	0.9821	0.1103	1.3703	0.9358
KITTI [21]	PointPWC-Net [36]	0.0694	0.7281	0.8884	0.2648	3.0062	0.7673
	RMS-FlowNet [1]	0.0530	0.8180	0.9380	0.2030	-	-
	HCRF-Flow [16]	0.0531	0.8631	0.9444	0.1797	2.0700	0.8656
	PV-RAFT [34]	0.0560	0.8226	0.9372	0.2163	-	-
	FlowStep3D [15]	0.0546	0.8051	0.9254	0.1492	-	-
	RCP [10]	0.0481	0.8491	0.9448	0.1228	-	-
	Bi-PointFlowNet [3]	0.0300	0.9200	0.9600	0.1410	1.0560	0.9490
	3DFlow [29]	0.0309	0.9047	0.9580	0.1612	1.1285	0.9451
	Ours	0.0277	0.9209	0.9613	0.1350	0.9773	0.9574

Table 1. **Quantitative results on FlyingThings3D and KITTI Scene Flow 2015 datasets.** All listed approaches are only trained on FlyingThings3D dataset in a fully-supervised manner. The best results are marked in bold.

3.5. Loss

The whole system is in a fully-supervised manner by using multi-scale loss \mathcal{L}_S the same as [1, 3, 36]. \mathcal{L}_S can be expressed as:

$$\mathcal{L}_S = \sum_{l=0}^L \gamma^l \sum_i \|\hat{s}^l - s_{gt}^l\|_2 \quad (17)$$

where γ^l represents the weight for each pyramid layer l . The predicted scene flow is denoted by \hat{s}^l . And $\|\cdot\|_2$ refers to the L_2 -norm.

In order to conduct the weight-sharing aggregation constraints, we use \mathcal{L}_P loss to constrain the weight indirectly by converging the aggregated coordinates to the real coordinates.

$$\mathcal{L}_P = \sum_{l=0}^L \gamma^l \sum_i \|\hat{p}^l - p_{gt}^l\|_2 \quad (18)$$

where \hat{p}^l represents the aggregated coordinates.

Besides, we introduce a deformation degree loss \mathcal{L}_{DD} to keep the geometry as much as possible during point clouds are moving. \mathcal{L}_{DD} can be expressed as:

$$\mathcal{L}_{DD} = \sum_{l=0}^L \gamma^l \sum_i \|\delta_{DD}^l\|_2 \quad (19)$$

where δ_{DD}^l indicates the deformation degree module.

The overall loss \mathcal{L}_{all} comprises \mathcal{L}_S , \mathcal{L}_P and \mathcal{L}_{DD} .

$$\mathcal{L}_{all} = \alpha_S \mathcal{L}_S + \alpha_P \mathcal{L}_P + \alpha_{DD} \mathcal{L}_{DD} \quad (20)$$

where α_S , α_P and α_{DD} are the weights for each term.

4. Experiments

In this section, we first introduce the datasets and evaluation metrics (§ 4.1). Next, we show the experimental setup (§ 4.2). Then we evaluate comparison with other networks (§ 4.3) to verify the effectiveness and generalization capability of our method. Finally, in the ablation study (§ 4.4), we evaluate and analyze the design of our methods.

4.1. Datasets and Evaluation Metrics

Datasets. To verify the effectiveness of our method, we use the synthetic dataset FlyingThings3D [19] and real scene dataset KITTI Scene Flow 2015 [21] the same as previous methods. FlyingThings3D dataset contains 19,640 pairs in training set and 3,824 pairs in the test set. We follow HPLFlowNet [12] to preprocess data. Utilizing the disparity and optical flow to generate point clouds data and remove the points with depth larger than 35m. KITTI dataset contains 200 pairs in training set and 200 pairs in the test set. we also preprocess the dataset following HPLFlowNet [12] and generate 142 pairs point clouds in the training set, because the disparity of the test set is not available. Ground points (height<0.3m) are removed.

Evaluation Metrics. For fair comparison, we evaluate the scene flow by following metrics, the same as [1, 3, 36].

- *EPE3D*: $\left\| \hat{S}^l - S_{gt}^l \right\|_2$ averaged end point error over each point in meters.

- *Acc3DS*: the percentage of points with *EPE3D* < 0.05m or relative error < 5%.

- *Acc3DR*: the percentage of points with *EPE3D* < 0.1m

MN	DD	WSA	EPE3D(m)↓	Acc3D Strict↑	Acc3D Relax↑	Outliers3D↓	EPE2D↓	Acc2D↑
✓			0.0282	0.9308	0.9799	0.1317	1.7321	0.9273
✓	✓		0.0279	0.9264	0.9786	0.1410	1.6202	0.9223
✓		✓	0.0243	0.9387	0.9819	0.1162	1.3868	0.9358
✓	✓	✓	0.0239	0.9391	0.9821	0.1103	1.3703	0.9358

Table 2. **Ablation studies on FlyingThings3D dataset.** We list the various designs made up of different modules which we propose. “MN” denotes modified network. “DD” denotes deformation degree module. “WSA” denotes weight-sharing aggregation module. “✓” denotes using this module. The best results are marked in bold.

Method	Parameter (M)	Flops (G)	Runtime (ms)
PointPWC-Net [36]	7.7	14.4	77.5
Bi-PointFlowNet [3]	7.9	13.3	82.5
3DFlow [29]	4.8	24.1	53.8
3DFlow [29](change)	4.8	25.6	127.8
Ours	3.7	15.5	86.4

Table 3. **Computational resource consumption and Runtime.** The results are evaluated on a single NVIDIA RTX 3090 GPU.

or relative error $< 10\%$.

- *Outliers3D*: the percentage of points with $EPE3D > 0.3m$ or relative error $> 10\%$.
- *EPE2D*: 2D average end point error obtained by projecting back to the image plane.
- *Acc2D*: the percentage of points whose $EPE2D < 3px$ or relative error $< 5\%$.

4.2. Experimental Setup

We conduct experiments on NVIDIA RTX 3090 GPUs. We train on the FlyingThings3D training dataset. The inputs of our network are only two frame point coordinates and the input size is 8192 by randomly sampling. To speed up, the training process is divided into two stages. We first train our model on a quarter of the training set (4910 pairs), then fine-tune on the whole training set. In the first stage, the learning rate is set to 0.001 and the decay rate is 0.7 for every 20 epochs. Pre-training is done for 80 epochs. In the second stage, the learning rate is set to 0.000343 and the decay rate is the same as before. Fine-tuning is done for 160 epochs after loading the pre-trained model. The parameters of Adam optimizer are set to $\beta_1 = 0.9$, $\beta_2 = 0.99$, $weight_decay = 0.0001$. The weights γ^l of loss are set to be $\gamma^0 = 0.02$, $\gamma^1 = 0.04$, $\gamma^2 = 0.08$, $\gamma^3 = 0.16$ and $\gamma^4 = 0.16$. We evaluate on the FlyingThings3D test dataset to demonstrate the effectiveness. In addition, to verify the generalization capability of our method, we test the model on the KITTI dataset without fine-tuning.

4.3. Main Results

We compare with the published state-of-the-art methods on the FlyingThings3D [19] and KITTI Scene Flow 2015 [21] datasets, the quantitative results are shown in Tab. 1. Among the methods listed, HCRF-Flow [16] only trained on a quarter of the FlyingThings3D training dataset. Others trained on the complete training dataset. RMS-FlowNet [1] adopts Random-sampling mechanism for multi-layer. Others adopt Farthest-Point-Sampling mechanism. Besides, different from others evaluating 8192 points’ scene flow results, 3DFlow [29] only evaluates 2048 points’.

On FlyingThings3D dataset, our method outperforms prior SOTA work on all evaluation metrics, which proves the effectiveness of our method. Our method surpasses current SOTA method Bi-PointFlowNet [3] by 14.6% on EPE3D metric. We surpass HCRF-Flow [16] which utilizes the direct rigidity constraints by 51.0% on EPE3D metric.

On KITTI Scene Flow 2015 dataset, we evaluate our model without fine-tuning to verify the generalization ability. Our method outperforms prior SOTA method Bi-PointFlowNet [3] by 7.6% on EPE3D metric.

In Fig. 4, the visualization results demonstrate the better accuracy of our method than recent SOTA methods [3, 29] on FlyingThings3D and KITTI Scene Flow 2015 datasets. We also show the local details for easy observation. In some challenging areas, we still achieved good results (fewer red points means fewer errors).

4.4. Ablation Studies

Tab. 2 presents the results of different designs. We will analyze the effectiveness of each module we proposed in detail as follows.

Modified network. As shown in the first row of Tab. 2, the modified network we proposed (MN) outperforms the baseline network PointPWC-Net [36] and RMS-FlowNet [1] by a large margin.

Deformation degree module. We compared the results with and without deformation degree module. Equipping the module on the modified network structure can improve the performance. Even in outstanding designs (MN + WSA), there is still performance improvement by using de-

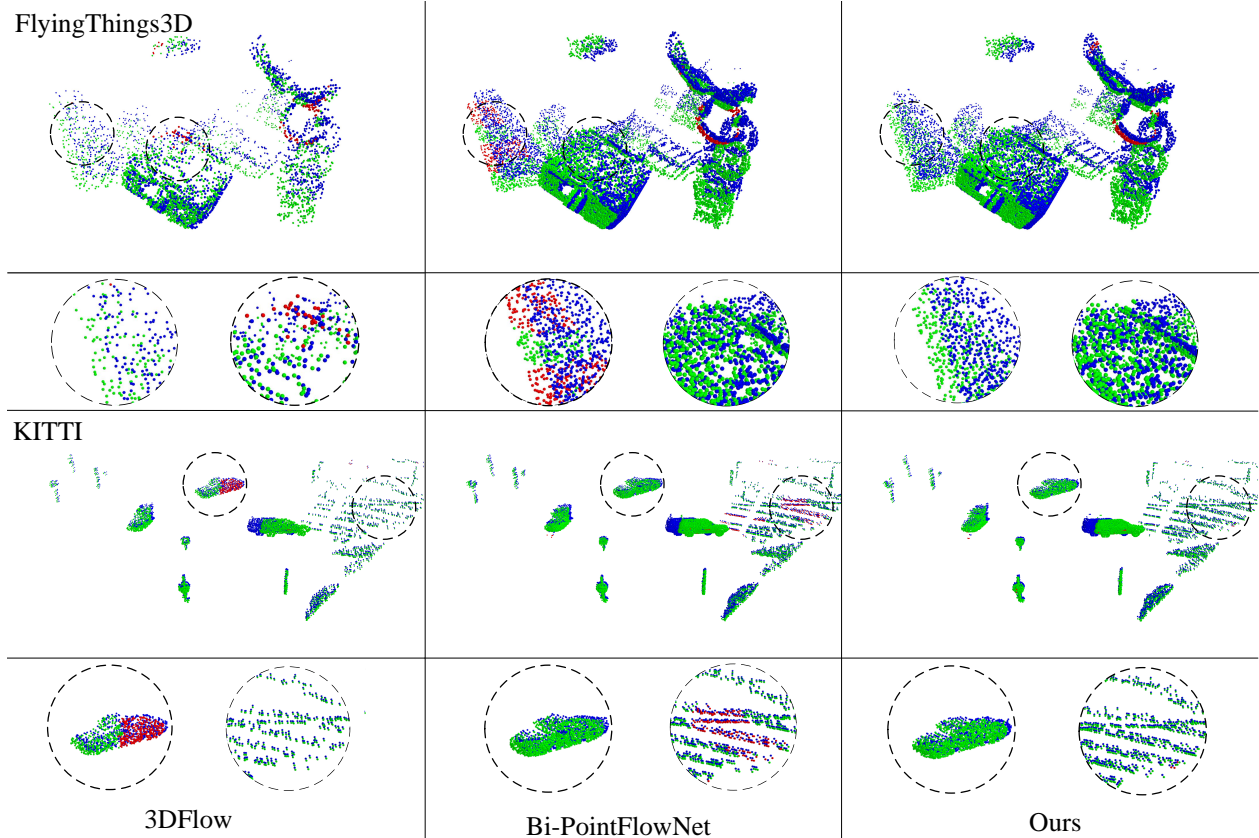


Figure 4. **Visualization Results.** From left to right: 3DFlow, Bi-PointFlowNet and our method. The first two rows are the experimental results on FlyingThings3D dataset. The last two rows are the experimental results on KITTI dataset. Blue: source point. Green: the correct warped source point by predicted scene flow according to *Acc3DS* metric. Red: the wrong warped source point by predicted scene flow according to *Acc3DS* metric.

formation degree module (MN + DD + WSA). Therefore, preserving local structure can obtain more accurate scene flow.

Weight-sharing aggregation. Contrast of the results of the first (MN) and third rows (MN + WSA) illustrates that adding a weight-sharing aggregation module can bring 13.8% accuracy improvement on EPE3D metric. It proves the validity of the weight-sharing aggregation constraints which use identical weights for aggregation of point coordinates, scene flow and features. It is consistent with the previous formula derivation conclusion (§ 3.2).

According to the analysis of the experimental results of the above different designs, each module we proposed is effective. The best method design consists of three modules (MN + DD + WSA).

4.5. Computational resource consumption and Runtime

We compare computational resource consumption and runtime with the prior SOTA methods. Note that 3DFlow

[29] only evaluates 2048 points’ experimental result, others test 8192 points for each frame. For fair comparison, we change the network of 3DFlow in order to predict 8192 points’ scene flow the same as others, which denoted by 3DFlow(change). The results show that the parameters of our methods are the least. On Flops and runtime metrics, we achieve comparable results with other methods.

5. Conclusion

In this paper, we propose weights-sharing aggregation constraints to employ the rigidity constraints indirectly, which avoids the errors caused by combining with other 3D tasks. Weights-sharing aggregation constraints align the aggregated weights of feature and scene flow with the aggregated weights of point coordinate. We prove the effectiveness of the constraints by formula derivation and experiments. In addition, we further keep the local geometric structure invariance by constructing the deformation degree module, which represents the structural difference in local areas between the source domain and the target domain.

It also provides geometric information for the subsequent estimator to obtain more precise scene flow. We modify the coarse-to-fine network and equip it with the module we proposed above. Experiments performed on the FlyingThings3D and KITTI scene flow datasets illustrate the effectiveness and generalization capability of our WSAFlowNet.

References

- [1] Ramy Batraway, René Schuster, Mohammad–Ali Nikouei Mahani, and Didier Stricker. Rms-flownet: Efficient and robust multi-scale scene flow estimation for large-scale point clouds. In *2022 International Conference on Robotics and Automation (ICRA)*, pages 883–889, 2022.
- [2] Aseem Behl, Despoina Paschalidou, Simon Donne, and Andreas Geiger. Pointflownet: Learning representations for rigid motion estimation from point clouds. In *Proceedings of the IEEE/CVF Conference on Computer Vision and Pattern Recognition (CVPR)*, June 2019.
- [3] Wencan Cheng and Jong Hwan Ko. Bi-pointflownet: Bidirectional learning for point cloud based scene flow estimation. In *European Conference on Computer Vision*, pages 108–124. Springer, 2022.
- [4] Cheng Chi, Qingjie Wang, Tianyu Hao, Peng Guo, and Xin Yang. Feature-level collaboration: Joint unsupervised learning of optical flow, stereo depth and camera motion. In *Proceedings of the IEEE/CVF Conference on Computer Vision and Pattern Recognition*, pages 2463–2473, 2021.
- [5] Marco Cuturi. Sinkhorn distances: Lightspeed computation of optimal transport. *Advances in neural information processing systems*, 26, 2013.
- [6] David Deng and Avideh Zakhori. Rsf: Optimizing rigid scene flow from 3d point clouds without labels. In *Proceedings of the IEEE/CVF Winter Conference on Applications of Computer Vision*, pages 1277–1286, 2023.
- [7] Guanting Dong, Yueyi Zhang, Hanlin Li, Xiaoyan Sun, and Zhiwei Xiong. Exploiting rigidity constraints for lidar scene flow estimation. In *Proceedings of the IEEE/CVF Conference on Computer Vision and Pattern Recognition (CVPR)*, pages 12776–12785, June 2022.
- [8] Martin Ester, Hans-Peter Kriegel, Jörg Sander, Xiaowei Xu, et al. A density-based algorithm for discovering clusters in large spatial databases with noise. In *kdd*, volume 96, pages 226–231, 1996.
- [9] Zan Gojcic, Or Litany, Andreas Wieser, Leonidas J. Guibas, and Tolga Birdal. Weakly supervised learning of rigid 3d scene flow. In *Proceedings of the IEEE/CVF Conference on Computer Vision and Pattern Recognition (CVPR)*, pages 5692–5703, June 2021.
- [10] Xiaodong Gu, Chengzhou Tang, Weihao Yuan, Zuozhuo Dai, Siyu Zhu, and Ping Tan. Rcp: Recurrent closest point for point cloud. In *Proceedings of the IEEE/CVF Conference on Computer Vision and Pattern Recognition (CVPR)*, pages 8216–8226, June 2022.
- [11] Xiuye Gu, Yijie Wang, Chongruo Wu, Yong Jae Lee, and Panqu Wang. Hplflownet: Hierarchical permutohedral lattice flownet for scene flow estimation on large-scale point clouds. In *Proceedings of the IEEE/CVF conference on computer vision and pattern recognition*, pages 3254–3263, 2019.
- [12] Xiuye Gu, Yijie Wang, Chongruo Wu, Yong Jae Lee, and Panqu Wang. Hplflownet: Hierarchical permutohedral lattice flownet for scene flow estimation on large-scale point clouds. In *Computer Vision and Pattern Recognition (CVPR), 2019 IEEE International Conference on*, 2019.
- [13] Gao Huang, Zhuang Liu, Laurens Van Der Maaten, and Kilian Q Weinberger. Densely connected convolutional networks. In *Proceedings of the IEEE conference on computer vision and pattern recognition*, pages 4700–4708, 2017.
- [14] Wolfgang Kabsch. A solution for the best rotation to relate two sets of vectors. *Acta Crystallographica Section A: Crystal Physics, Diffraction, Theoretical and General Crystallography*, 32(5):922–923, 1976.
- [15] Yair Kittenplon, Yonina C. Eldar, and Dan Raviv. Flowstep3d: Model unrolling for self-supervised scene flow estimation. In *Proceedings of the IEEE/CVF Conference on Computer Vision and Pattern Recognition (CVPR)*, pages 4114–4123, June 2021.
- [16] Ruibo Li, Guosheng Lin, Tong He, Fayao Liu, and Chunhua Shen. Hcrf-flow: Scene flow from point clouds with continuous high-order crfs and position-aware flow embedding. In *Proceedings of the IEEE/CVF Conference on Computer Vision and Pattern Recognition (CVPR)*, pages 364–373, June 2021.
- [17] Xingyu Liu, Charles R. Qi, and Leonidas J. Guibas. Flownet3d: Learning scene flow in 3d point clouds. In *Proceedings of the IEEE/CVF Conference on Computer Vision and Pattern Recognition (CVPR)*, June 2019.
- [18] D Man and A Vision. A computational investigation into the human representation and processing of visual information. *WH San Francisco: Freeman and Company, San Francisco*, 1982.
- [19] Nikolaus Mayer, Eddy Ilg, Philip Hausser, Philipp Fischer, Daniel Cremers, Alexey Dosovitskiy, and Thomas Brox. A large dataset to train convolutional networks for disparity, optical flow, and scene flow estimation. In *Proceedings of the IEEE Conference on Computer Vision and Pattern Recognition (CVPR)*, June 2016.
- [20] Moritz Menze and Andreas Geiger. Object scene flow for autonomous vehicles. In *Proceedings of the IEEE Conference on Computer Vision and Pattern Recognition (CVPR)*, June 2015.
- [21] Moritz Menze, Christian Heipke, and Andreas Geiger. Object scene flow. *ISPRS Journal of Photogrammetry and Remote Sensing*, 140:60–76, 2018.
- [22] Jean-Philippe Pons, Renaud Keriven, and Olivier Faugeras. Multi-view stereo reconstruction and scene flow estimation with a global image-based matching score. *International Journal of Computer Vision*, 72(2):179–193, 2007.
- [23] Jhony Kaesemodel Pontes, James Hays, and Simon Lucey. Scene flow from point clouds with or without learning. In *2020 International Conference on 3D Vision (3DV)*, pages 261–270, 2020.
- [24] Gilles Puy, Alexandre Boulch, and Renaud Marlet. Flot: Scene flow on point clouds guided by optimal transport. In

- European conference on computer vision*, pages 527–544. Springer, 2020.
- [25] Charles R Qi, Hao Su, Kaichun Mo, and Leonidas J Guibas. Pointnet: Deep learning on point sets for 3d classification and segmentation. In *Proceedings of the IEEE conference on computer vision and pattern recognition*, pages 652–660, 2017.
- [26] Charles Ruizhongtai Qi, Li Yi, Hao Su, and Leonidas J Guibas. Pointnet++: Deep hierarchical feature learning on point sets in a metric space. *Advances in neural information processing systems*, 30, 2017.
- [27] Julian Quiroga, Thomas Brox, Frédéric Devernay, and James Crowley. Dense semi-rigid scene flow estimation from rgbd images. In *European Conference on Computer Vision*, pages 567–582. Springer, 2014.
- [28] Huihsin Tseng, Pi-Chuan Chang, Galen Andrew, Dan Jurafsky, and Christopher D Manning. A conditional random field word segmenter for sighthan bakeoff 2005. In *Proceedings of the fourth SIGHAN workshop on Chinese language Processing*, 2005.
- [29] Guangming Wang, Yunzhe Hu, Zhe Liu, Yiyang Zhou, Masayoshi Tomizuka, Wei Zhan, and Hesheng Wang. What matters for 3d scene flow network. In *European Conference on Computer Vision*, pages 38–55. Springer, 2022.
- [30] Guangming Wang, Xinrui Wu, Zhe Liu, and Hesheng Wang. Hierarchical attention learning of scene flow in 3d point clouds. *IEEE Transactions on Image Processing*, 30:5168–5181, 2021.
- [31] Haiyan Wang, Jiahao Pang, Muhammad A. Lodhi, Yingli Tian, and Dong Tian. Festa: Flow estimation via spatial-temporal attention for scene point clouds. In *Proceedings of the IEEE/CVF Conference on Computer Vision and Pattern Recognition (CVPR)*, pages 14173–14182, June 2021.
- [32] Zirui Wang, Shuda Li, Henry Howard-Jenkins, Victor Prisacariu, and Min Chen. Flownet3d++: Geometric losses for deep scene flow estimation. In *Proceedings of the IEEE/CVF winter conference on applications of computer vision*, pages 91–98, 2020.
- [33] Andreas Wedel, Thomas Brox, Tobi Vaudrey, Clemens Rabe, Uwe Franke, and Daniel Cremers. Stereoscopic scene flow computation for 3d motion understanding. *International Journal of Computer Vision*, 95(1):29–51, 2011.
- [34] Yi Wei, Ziyi Wang, Yongming Rao, Jiwen Lu, and Jie Zhou. Pv-raft: Point-voxel correlation fields for scene flow estimation of point clouds. In *Proceedings of the IEEE/CVF Conference on Computer Vision and Pattern Recognition (CVPR)*, pages 6954–6963, June 2021.
- [35] Wenxuan Wu, Zhongang Qi, and Li Fuxin. Pointconv: Deep convolutional networks on 3d point clouds. In *Proceedings of the IEEE/CVF Conference on Computer Vision and Pattern Recognition (CVPR)*, June 2019.
- [36] Wenxuan Wu, Zhi Yuan Wang, Zhuwen Li, Wei Liu, and Li Fuxin. Pointpwc-net: Cost volume on point clouds for (self-) supervised scene flow estimation. In *European Conference on Computer Vision*, pages 88–107. Springer, 2020.
- [37] Zi Jian Yew and Gim Hee Lee. Rpm-net: Robust point matching using learned features. In *Proceedings of the IEEE/CVF Conference on Computer Vision and Pattern Recognition (CVPR)*, June 2020.
- [38] Guangyao Zhai, Xin Kong, Jinhao Cui, Yong Liu, and Zhen Yang. Flowmot: 3d multi-object tracking by scene flow association. *arXiv preprint arXiv:2012.07541*, 2020.